5.2

MESOSCALE CONVECTIVE VORTICES OBSERVED DURING BAMEX PART II: INFLUENCES ON CONVECTION INITIATION

S. B. Trier, and C. A. Davis

National Center for Atmospheric Research
Boulder, Colorado

1. INTRODUCTION

Part I (Davis and Trier 2004) presented a description of midtropospheric vortices generated by deep convection (MCVs) during the Bow-Echo and MCV Experiment (BAMEX). The internal flow and thermodynamic structure of three of the five MCVs sampled at maturity was analyzed. In this paper we extend our analysis of these three cases, focusing on the relationship between MCV structure and heavy precipitation.

Much of the meteorological interest in MCVs stems from from their ability to focus the location of heavy precipitation. Climatological studies (Bartels and Maddox 1991; Trier et al. 2000, Davis et al. 2002) have indicated that the redevelopment of deep convection commonly occurs in close proximity to MCVs. Thus, when present, MCVs constitute an important component of the warm season precipitation forecast problem. Figure 1 compares forecasts of deep convection from the NCEP Eta operational model and an experimental version of the Weather Research and Forecasts (WRF) model that was run for the BAMEX region (see, e.g., Davis and Weisman 2004). The WRF model (Fig. 1b) produces a superior forecast of afternoon convection in eastern Kansas on 29 June 2003 (BAMEX IOP 15) when compared with observations (Fig. 1c). The Eta model produces heavy precipitation, but several hundreds of km too far west in western Kansas (Fig. 1a). The failure of the Eta forecast in this case is attributed to its inability to capture the observed MCV circulation, which, as we shall see, has a large influence on the thermodynamic stability of the environment in which deep convection forms.

One mechanism by which MCVs influence convection initiation is their interaction with the environmental vertical shear in which they are embedded. Raymond and Jiang (1990) idealized MCVs as potential vorticity anomalies with balanced temperature and vertical vorticity fields and noted that the lower-tropospheric vertical motion pattern associated with a steady, balanced vortex embedded in environmental vertical shear would be one of isentropic ascent (descent) on its downshear (upshear) side (Fig. 2a). They argued further that there would be additional isentropic vertical motion associated with the tangential component of the flow within a baroclinic vortex (Fig. 2b). Trier and Davis (2002) confirmed that balanced lifting contributed substantially to

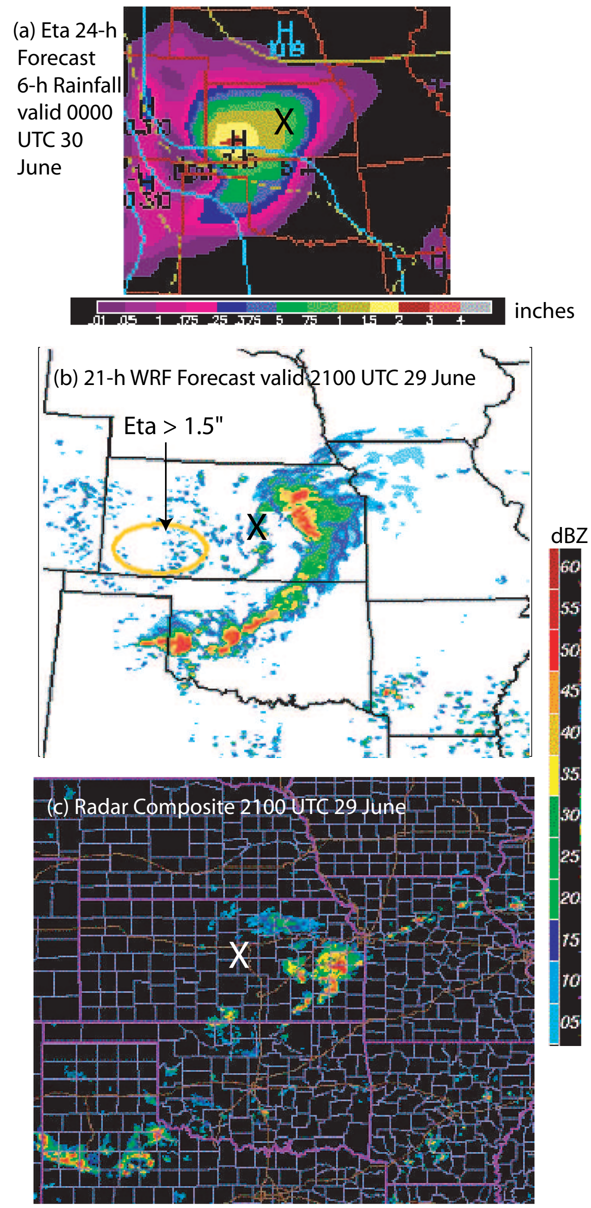

Figure 1. (a) 24-h forecast of 6-h accumulated rainfall (inches) from the NCEP Eta model valid 0000 UTC 30 June 2003, (b) 21-h forecast of model-derived radar reflectivity (dBZ) from the WRF model valid 2100 UTC 29 June 2003, and (c) composite map of observed radar reflectivity at 2100 UTC 29 June 2003. The X symbol on each panel represents the approximate location of the observed MCV center at 2100 UTC 29 June 2003.

Corresponding author address: Dr. Stanley B. Trier, National Center for Atmospheric Research, P.O. Box 3000, Boulder CO 80307-3000

the direct production of heavy precipitation by cooling and eventually saturating lower-tropospheric air parcels originating near the top of the planetary boundary layer (PBL). In other cases, MCV-induced vertical motions and horizontal advections may simply provide a focus by predisposing certain locations to deep convection, which is directly initiated by other mechanisms.

The copious sounding data gathered during BAMEX (e.g., Davis and Weisman 2004; Ahijevych et al. 2004) provide an opportunity to examine the relationship between the MCV circulation and heavy precipitation in unprecedented detail. The three BAMEX cases introduced in part I comprised MCVs of differing strength that occurred in environments of differing environmental vertical shear and thermodynamic stability. Despite these differences, heavy precipitation was observed within 200 km of the MCV circulation at the composite analysis (see discussion in part I, section 2) times in each of the three cases. In this study we document how large variability in thermodynamic stability and vertical shear occurs across the MCV circulation and examine mechanisms that account for the differences in these parameters which modulate the structure and intensity of MCV-induced precipitation.

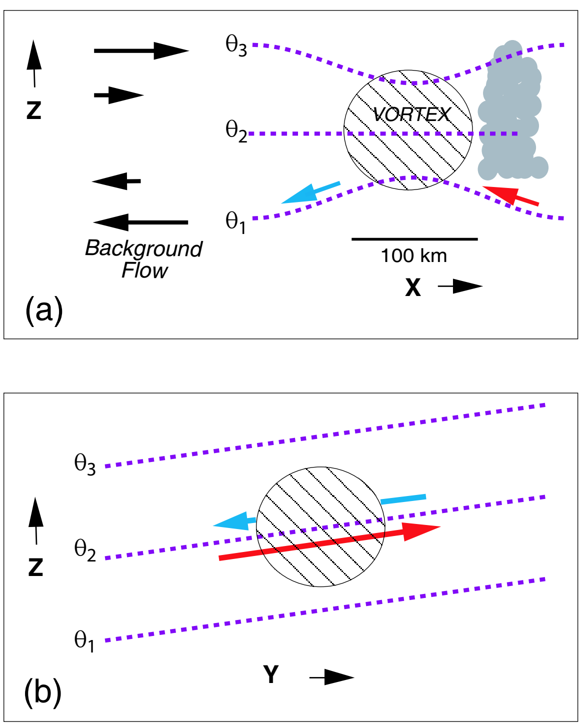

Figure 2. Schematic diagram illustrating quasi-balanced lifting in the vicinity of a positive PV anomaly (hatched) in ambient vertical shear. (a) Upglide associated with the background vertical shear along isentropic surfaces deformed by the vortex, and (b) vortex-induced motion along the isentropic surfaces of the background baroclinic zone. Reproduced from Trier et al. (2000), based on Fig. 2 of Raymond and Jiang (1990).

2. ENVIRONMENTAL SHEAR

The vertical shear associated with MCVs results from both the MCV circulation and the larger-scale environment in which it's embedded. While local organization of deep convection within the MCV circulation is sensitive to the total vertical shear, the mesoscale vertical motions discussed in the introduction are most influenced by the environmental vertical shear within a layer from above the surface to the approximate level of the midtropospheric vortex center (e.g., Fig. 2). Assuming the vortex is relatively symmetric, we estimate the background shear from averages of dropsonde and profiler winds on horizontal pressure surfaces that span the horizontal extent of the MCV circulation (Fig. 3).

Vertical shear is calculated for the 300-hPa layer starting approximately 50-hPa above the surface. The background vertical shear is primarily westerly, ranging from azimuth 300° in IOP 1 to azimuth 255° in IOP 15, but varies strongly in magnitude for each case (Fig. 3). In IOP 1 the environmental vertical shear from 900 to 600 hPa of $|\triangle\mathbf{v}| = 15.7$ m s^{-1} (Fig. 3a) is the strongest for any MCV case during BAMEX, whereas $|\triangle\mathbf{v}| = 1.0$ m s^{-1} in IOP 8 (Fig. 3b) is the weakest for all BAMEX MCV cases. The environmental vertical shear magnitude from 850 to 550 hPa of 7.8 m s^{-1} for IOP 15 (Fig. 3c) constitutes an intermediate value for BAMEX MCV cases.

3. VERTICAL MOTIONS IN THE VICINITY OF THE MCVS

Lower-tropospheric vertical velocity, $\omega = Dp/Dt$, is calculated kinematically by vertical integration of the horizontal divergence valid at the centroids of triangles discussed in part I. The 700-hPa ω fields are then subjectively analyzed and displayed with the 700-hPa MCV-relative horizontal flow and radar reflectively at the composite analysis time for IOP 1 (Fig. 4a), IOP 8 (Fig. 5a), and IOP 15 (Fig. 6a).

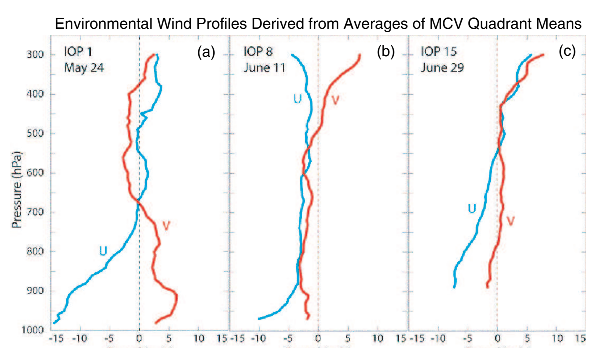

Figure 3. Estimated environmental wind profiles (m s^{-1}) based on an average of quadrant (i.e., NE, SE, SW, NW) means obtained from dropsonde and profiler data within 300 km of the MCV center for BAMEX IOPs (a) 1 (24 May 2003), (b) 8 (11 June 2003), and (c) 15 (29 June 2003).

In IOP 1 a widespread and persistent shield of heavy stratiform precipitation is located from ∼50 km west of the MCV center to the eastern flank of the circulation ∼150 km to its east (Fig. 4a). Upward motion occurs near the MCV center with maximum ascent in excess of -15 μb s^{-1} slightly downshear. A region of weak descent (ω ∼5 μb s^{-1}) is located on the northwestern edge of the precipitation area, upshear from the circulation center. The relatively large magnitude and location of maximum ascent downshear are consistent with the isentropic lifting (Fig. 2) associated with a vortex of moderate strength in strong vertical shear (Fig. 3a). However, the overall predominance of ascent within the MCV circulation, and its significant magnitude at the vortex center, suggests the possibility of some modification of the vertical motion resulting from latent heat release in the widespread heavy precipitation.

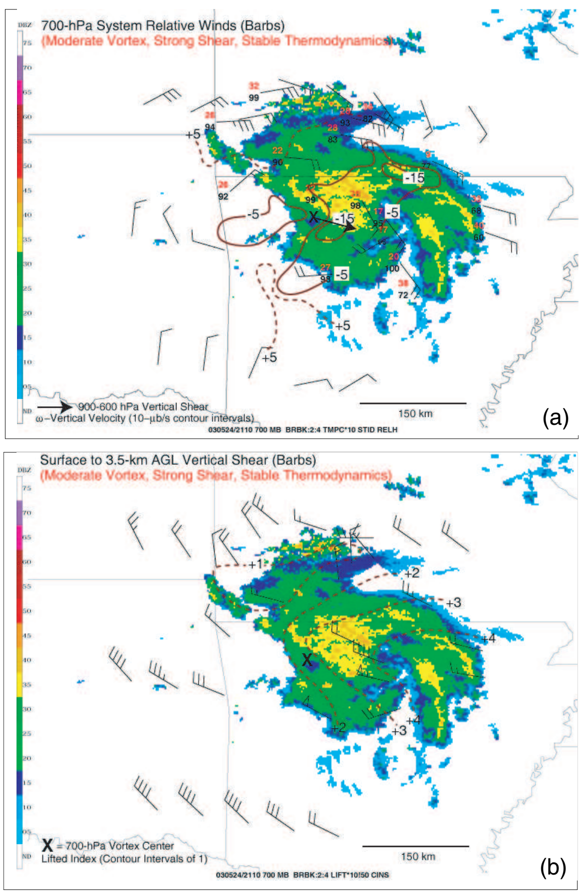

Figure 4. 2110 UTC 24 May 2003 (BAMEX IOP 1) composite analysis of radar reflectivity (colors) and (a) 700-hPa system-relative horizontal winds (m s^{-1}; full barb = 5 m s^{-1}, half barb = 2.5 m s^{-1}), and ω vertical velocity (μb s^{-1}; no zero contour); and (b) 0-3.5 km AGL vertical shear (m s^{-1}; flag = 25 m s^{-1}, full barb = 5 m s^{-1}, half barb = 2.5 m s^{-1}) and lifted index (LI) based on 500 m-deep boundary layer air parcel (1°C contour interval). The arrow in part (a) schematically indicates environmental vertical shear direction. The **x** symbol in both panels indicates the estimated location of the 700-hPa MCV center.

In IOP 15 (Fig. 5a) the 700-hPa vertical motion pattern is more consistent with the Raymond and Jiang (1990) conceptual model of MCV-induced isentropic vertical motion. Here, the vertical motion pattern is characterized by a well-defined couplet of weak ascent (descent) magnitudes of 5 to 8 μb s^{-1} located downshear (upshear) from the MCV center. Note that the ascent extends from the southeastern quadrant of the vortex to just north of the vortex center, and is consistent with the warm temperature advection pattern (i.e., isentropic upglide) in Fig. 8 of part I.

Unlike in IOP 1, the precipitation in IOP 15 is highly convective and, while located predominately downshear, is most intense and widespread farther from the MCV center near the eastern edge of the 700-hPa upward vertical motion (Fig. 5a). This MCV is embedded within a weak E-W oriented larger-scale baroclinic zone, and scattered convection is also beginning to develop within the lower-tropospheric frontal zone in Missouri, significantly northeast of the MCV center. In addition, a E-W oriented band of lighter precipitation is located near the frontal zone on the northern periphery of the MCV circulation. The eastward extension of the upward motion on the northeastern margin of the MCV circulation (Fig. 5a) is likely enhanced by low-level horizontal convergence (beneath 700 hPa) within the northward sloping E-W oriented frontal zone (not shown).

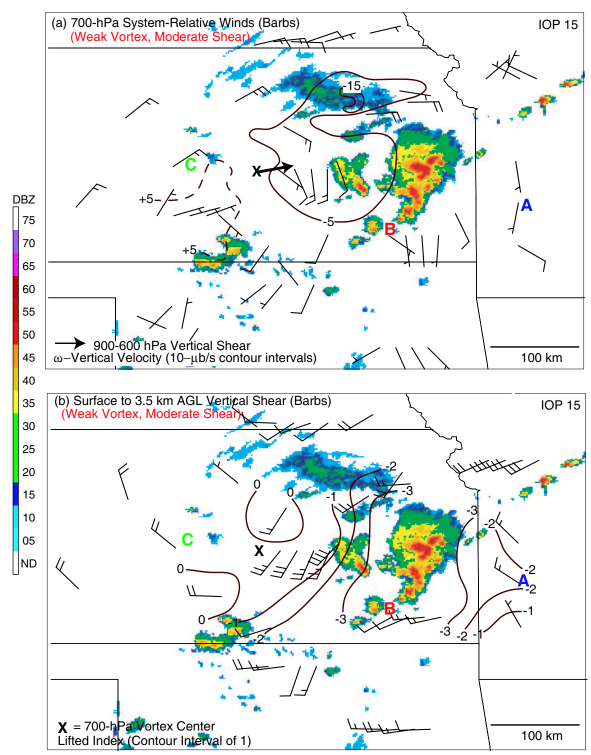

Figure 5. As in Fig. 4 but for 2050 UTC 29 June 2003 (BAMEX IOP 15). The annotations A, B, and C indicate the respective locations of the blue, red, and green sounding curves displayed in Fig. 9.

The IOP 8 MCV (Fig. 6a) is the largest and strongest MCV sampled in BAMEX. However, unlike in IOPs 1 and 15, this MCV occurred in an environment of nearly negligible vertical shear (Fig. 3). In this strong vortex/weak vertical shear regime, the 700-hPa vertical motion pattern exhibits considerable fine-scale structure with numerous centers of moderate-to-strong ascent and descent (Fig. 6a) instead of the single vertical motion dipole structure evident in IOP 15 (Fig. 5a). The precipitation pattern differs as well, with bands of intense convection on the southeast periphery of the MCV and weaker bands north of the MCV center and on the northwest flank of the MCV circulation (Fig. 6a).

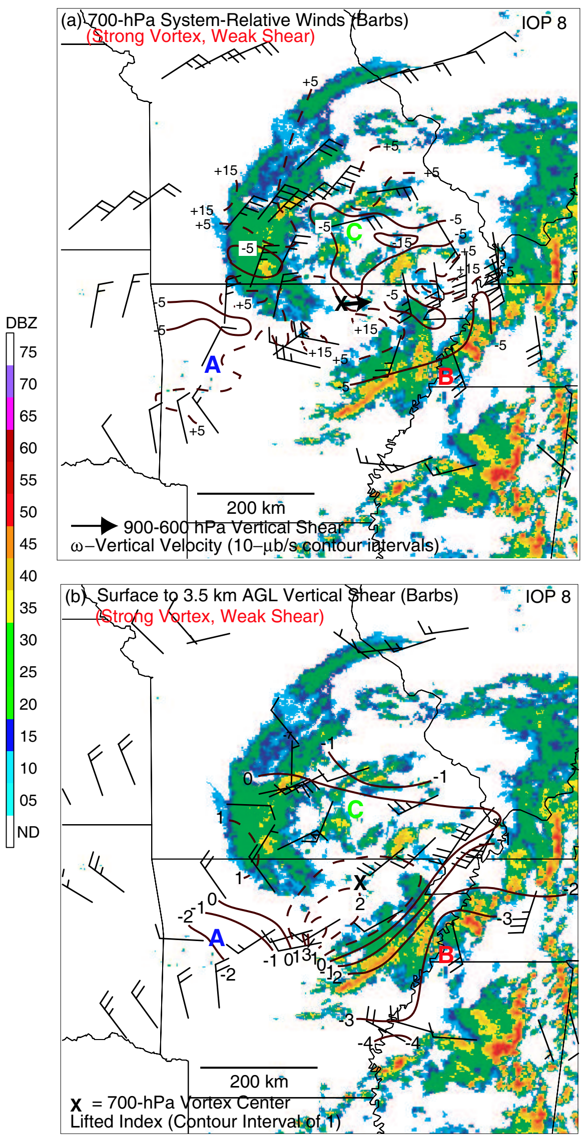

Figure 6. As in Fig. 4 but for 1730 UTC 11 June 2003 (BAMEX IOP 8). The annotations A, B, and C indicate the respective locations of the blue, red, and green sounding curves displayed in Fig. 11.

4. KINEMATIC AND THERMODYNAMIC INFLUENCES ON MCV PRECIPITATION

It is well known from past studies that the mesoscale variation in the thermodynamic vertical structure (e.g., moisture and instability) and flow structure (e.g., vertical shear, environmental vertical motion) can strongly influence the organization and intensity of deep convection. Thus it is reasonable to expect that differences in these structural characteristics may account for some of differences in the precipitation patterns among the three MCV cases discussed in the previous section.

Unlike IOPs 15 and 8, which featured intense convective precipitation on the southeast flank of the MCV, the IOP 1 MCV was characterized by persistent widespread stratiform precipitation closer to its center with embedded banded features of slightly enhanced reflectivity (Fig. 4b). The Lifted Index (LI) indicates thermodynamically stable conditions over the precipitation region with the most stable conditions for PBL-based air parcels (LI $>$ 4) at the eastern edge (Fig. 4b), in the direction toward which the MCV and its precipitation shield are moving. This suggests that the primary mechanism responsible for the production of precipitation in this case is the lifting of moist, but conditionally stable air to saturation by the MCV circulation (Fig. 4).

In both IOPs 15 and 8, the most intense convection occurs within the regions of greatest conditional instability in the composite analyses (Figs. 5b and 6b, respectively) where LIs are $<$ -2. In these cases the maximum conditional instability is located east and southeast of the strongest 700-hPa vertical motion (Figs. 5, 6). One of the reasons for the offset of the maximum conditional instability from the strongest dynamical forcing may be the general location of the upward motion maxima closer to the vortex center where warmer conditions in the middle and upper troposphere occur, consistent the MCVs' quasi-balanced thermal structure (part I). Daytime insolation is also reduced close to the MCV center due to midlevel cloudiness (Figs. 7 and 8) resulting in part from the lower-middle tropospheric ascent. The reduced insolation results in cooler boundary layer temperatures near the MCV center than farther east along its periphery. Conditionally stable conditions occur southwest of the MCV center in both IOP 15 (Fig. 5b) and IOP 8 (Fig. 6b), and are approximately collocated with regions of maximum 700-hPa descent (Figs. 5a and 6a).

The large horizontal variations in thermodynamic stability across the MCV in IOPs 15 and 8 in the composite LI analyses (Figs. 5b and 6b) may be better understood by examining selected dropsondes in different locations relative to the MCV center. Launch times of individual dropsondes may be offset by up to $\sim$ 90 min from the central composite analysis times. Thus, caution must be exercised when using these soundings to interpret the the effect of the local environment on the unsteady precipitation features depicted at the central time in the composite analyses. However, these soundings are expected to reliably convey differences in the general vertical thermodynamic and wind structure among the undisturbed environment and various quadrants of the analyzed MCVs, which we examine in the remainder of this section.

The conditionally unstable PBL of the undisturbed environment 300 km east of the MCV center in IOP 15 (point A in Fig. 5) is capped by a significant 850-hPa inversion with dry conditions aloft (Fig. 9, blue curves) that inhibit deep convection. This thermodynamic vertical structure contrasts with conditions about 75 west of the MCV center (point C in Fig. 5), which are up to 5°C cooler in the 700-850 hPa layer and are nearly saturated (Fig. 9, green curves). The much cooler conditions in this layer are consistent with a history of isentropic ascent implied by tangential upgliding flow around the vortex center (Fig. 8 of part I), inasmuch as the 700-hPa streamlines are a reasonable approximation of the horizontal component of actual air parcel trajectories in this slowly moving vortex. Examination of 6-h radar animations (not shown) indicated persistent stratiform precipitation in this location, which had mostly dissipated by the time of the composite analysis (Fig. 5). Thus the balanced contribution to cooling underneath the vortex in this location near its center may have been supplemented by diabatic processes such as evaporation of precipitation.

Along the southeastern periphery of the IOP 15 MCV (point B in Fig. 5), where the most intense convection initiates, the PBL is conditionally unstable (Fig. 9, red curves) with cooler and moister conditions immediately above the PBL than in the dry environment farther east. Lower-tropospheric mesoscale ascent (Fig. 5a) may partly account for the cooler conditions above the PBL, which facilitates convection initiation. Also important to convection initiation, is the much greater PBL moisture in this region (Fig. 9). A closed circulation is present in the 1900 UTC analysis of ground

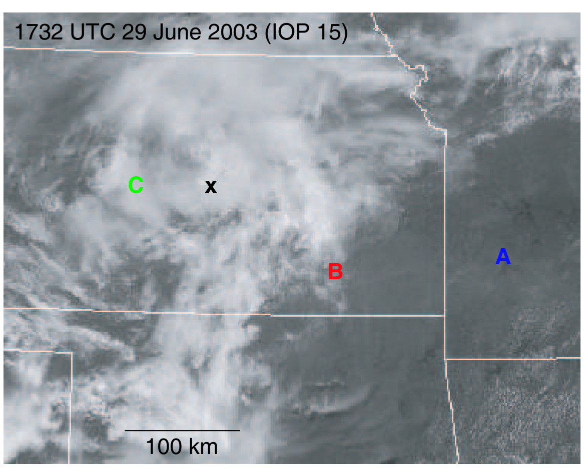

Figure 7. Visible satellite imagery at 1730 UTC 29 June 2003 prior to the redevelopment of deep convection in IOP 15. The **x** symbol marks the approximate MCV circulation center. The annotations A, B, and C indicate the respective locations of the blue, red, and green sounding curves displayed in Fig. 9.

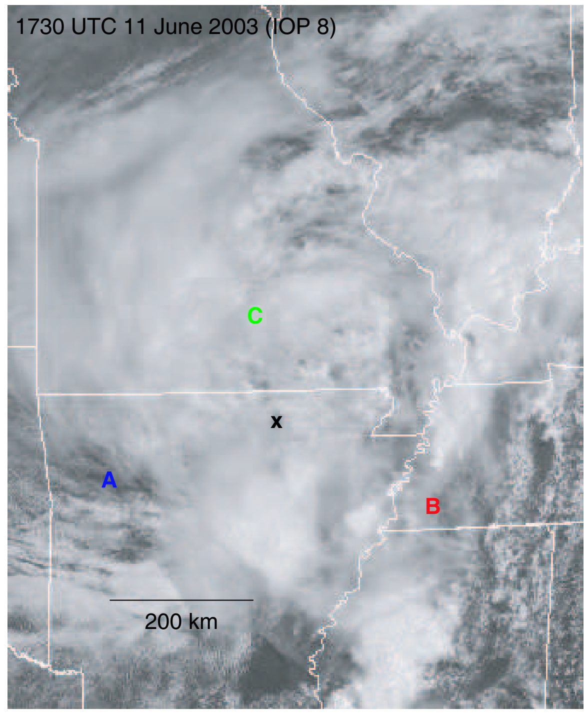

Figure 8. Visible satellite imagery at 1730 UTC 11 June 2003 which coincides with the central time of the IOP 8 composite analysis presented in Fig. 6. The **x** symbol marks the approximate MCV circulation center. The annotations A, B, and C indicate the respective locations of the blue, red, and green sounding curves displayed in Fig. 11.

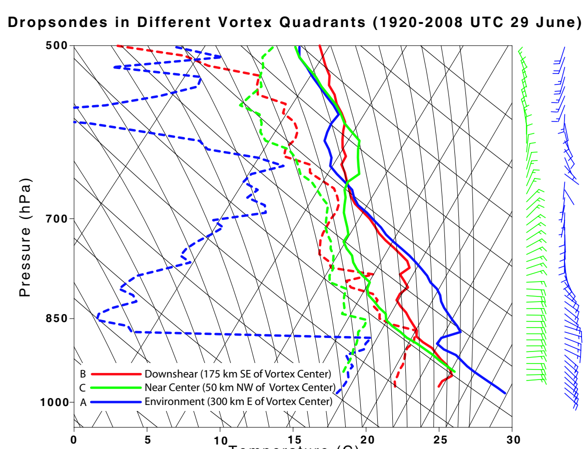

Figure 9. Dropsonde observations of temperature (solid lines), dew point (dashed lines), and system-relative horizontal winds (m s^{-1}) locations specifi ed by the annotations A (blue), B (Red), and C (Green), in the 2050 UTC 29 June IOP 15 composite analysis of Fig. 5.

relative surface wind (Fig. 10), however its center is shifted about 150 km ESE of the 700-hPa center (cf. Fig. 5a). By this time, the tangential flow on the east flank of the surface vortex had advected high equivalent potential temperature θ_e air originating from farther south and may have therefore contributed to the local maximum of θ_e (Fig. 10) and enhanced conditional instability on the southeast periphery of the MCV circulation where deep convection occurs (Fig. 5b).

Enhanced PBL moisture and warmer temperatures also occur along the southeast periphery of the larger and stronger IOP 8 MCV (Fig. 11, red curves), which again favors convection initiation in this portion of the MCV circulation (Fig. 6b, pt. B). A closed circulation is also evident at the surface in this MCV (not shown), suggesting that MCV-induced horizontal advections could be playing a role in thermodynamic destabilization as in IOP 15. Also similar to the IOP 15 case, conditions on the north side of the vortex (Fig. 6, pt. C) were much cooler both above and within the PBL (Fig. 11, green curves), which reflects the effects of mesoscale vertical motion (Fig. 6a) and reduced surface insolation from widespread cloudiness (Fig. 8), respectively. The nearly moist adiabatic lapse rate extending from the top of the shallow PBL into the middle troposphere in this location is similar to IOP 15, and contributes to the lack of significant conditional instability. Heavy rain

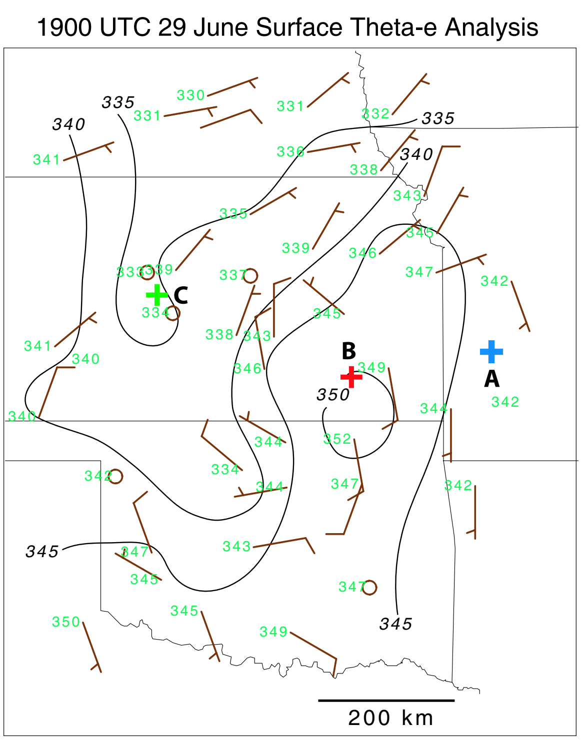

Figure 10. Ground-relative surface winds (knots) and analysis of surface equivalent potential temperature θ_e (5-K increments) for BAMEX IOP 15 at 1900 UTC 29 June 2003. The A, B, and C annotations refer to the locations of the color coded soundings in Fig. 9.

was intermittently present in this northern portion of the MCV circulation. However, the precipitation was largely stratiform with only weak embedded convective elements. Along the southwest periphery of this MCV (pt. A in Fig. 6), the sounding (Fig. 11, blue curves) possesses a strong dry inversion at 850 hPa, which explains the lack of deep convection despite conditional instability of the PBL (Fig. 11). The inversion itself is consistent with the implied 850-hPa isentropic descent on the southwest periphery of the MCV (Fig. 5, part I).

In addition to thermodynamic stability, strong horizontal variations in the vertical shear occur over the lowest 3.5 km across the MCVs. This is due to both differences in the MCV-induced vertical shear magnitude, which itself results from factors such as vortex tilt and differences in vortex intensity with height, and how this vertical shear superposes with the background vertical shear. The IOP 15 MCV is a good example of strong variation in vertical shear occurring across the vortex (Fig. 5b). In this case the background vertical shear is southwesterly (Fig. 3), so vortex-induced vertical shear enhances (reduces) the total vertical shear south and east (north and west) of the MCV center. In the IOP 8 case, the vertical shear on the southeast periphery of the MCV of 15-17.5 m s^{-1} over 3.5 km has a significant MCV-induced component, and when the resulting strong total vertical shear is combined with at least moderate conditional instability (LI $<$ -3), it is sufficient to produce severe squall line convection over western Tennessee (Fig. 6b).

5. SUMMARY AND DISCUSSION

In this study we have examined the precipitation patterns within three MCVs of varying strength, each occurring within differing environmental shear and thermodynamic stability regimes. In cases of moderate-to-strong vertical shear beneath the level of maximum vortex strength (IOPs 1 and 15), the instantaneous 700-

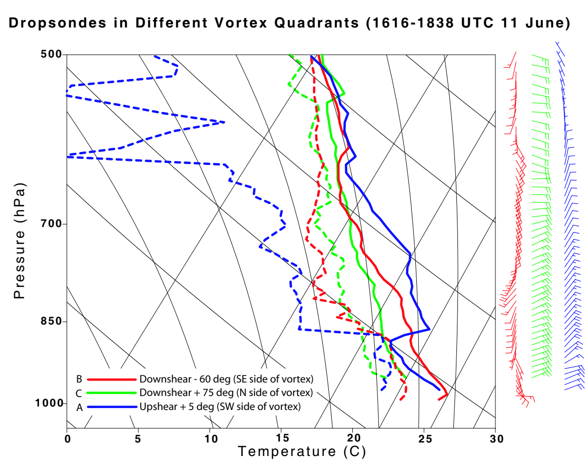

Figure 11. As in Fig. 9 but for the 1730 11 June IOP 8 composite analysis of Fig. 6.

hPa vertical motion pattern resembles the conceptual model of Raymond and Jiang (1990), which includes isentropic ascent (descent) downshear (upshear) of the MCV circulation center. However, in cases of weak environmental vertical shear (e.g., IOP 8), the observed vertical motion pattern is more complicated.

In each of the cases thermodynamic stabilization occurs in the wake (i.e., west and southwest) of the MCV, which corresponds to its upshear quadrants. This region is relatively precipitation free. In one of the cases (IOP 1), the MCV-induced lifting near its center appears sufficient to organize a widespread area of heavy precipitation in the absence of conditional instability. In the two other cases (IOPs 8 and 15), the heaviest precipitation occurs along the periphery of the MCV circulation where conditional instability is greatest. The effect of the mesoscale ascent (descent) within the MCV circulation in these cases is to increase (decrease) the conditional instability by cooling and moistening (warming and drying) the layer extending from the top of the PBL into the middle troposphere. However, the region of greatest conditional instability is determined not only by the vertical motions, which are greatest downshear near the MCV center (i.e., near or within the radius of maximum tangential winds), but also by low-level horizontal temperature and moisture advections and surface heating, which also occur downshear, but result in the greatest PBL θ_e increases farther from the MCV center.

In addition to enhancements in thermodynamic instability, vertical shear is also enhanced in parts of the MCV circulation. The character of shear enhancement depends on details of the vortex structure and its environment, and thus can vary significantly from case to case. Since the strength of the MCV circulation generally increases through the lower troposphere, and the background vertical shear is predominately westerly in the central United States warm season convective environment, enhanced westerly (southerly) shear is often found in the southern (eastern) quadrant of MCVs. The enhanced vertical shear supported severe convection within the MCV circulation of IOP 8, whereas in IOP 15, the greatest vertical shear enhancement occurred closer to the MCV center than did the region of greatest conditional instability where deep convection actually formed.

It should be noted that the relationships among the characteristics of the MCV circulation including its variations in vertical motion and thermodynamic stability and their effect on deep convection discussed above pertain to only three MCVs that were sampled during the early to late afternoon. The relative importance of the MCV-induced motions, differential heating, and various additional environmental factors are anticipated to be different in episodes of nocturnal convection that can occur with some of the largest and longest-lived MCVs (e.g., Fritsch et al. 1994; Trier and Davis 2002).

It is also true that we while have attempted to isolate the effects of the MCV circulation on deep convection in the current study, MCVs often occur in the presence of additional forcing mechanisms including horizontal convergence along synoptic fronts or convective outflows, which themselves may play an important role in convection initiation. For example, both the IOP 15 and IOP 5 (not shown) MCVs occurred within and above shallow, but more horizontally extensive, E-W oriented baroclinic zones. In these cases, the role of the MCV was likely to focus the region of most intense mesoscale vertical motions, within a preexisting favorable environment for deep convection. Further study is required to understand how additional factors in the mesoscale environment interact with the effects of the MCV-induced circulation to focus deep convection.

Because of their longevity and strong influence on mesoscale vertical motions and horizontal advection, it is, however, clear that adequate prediction of MCVs are important to successful operational forecasts of deep convection in subsequent diurnal cycles. Since MCVs generally form in regions of vertical gradients of diabatic heating within large MCSs, we are optimistic that the next generation of operational forecast models (including the WRF, Fig. 1b), which have the capability to explicitly resolve deep convection, may become potentially useful tools for successful prediction of MCV-related convection.

REFERENCES

Ahijevych, D. A., G. Bryan, C. A. Davis, J. C. Knievel, S. B. Trier, M. Weisman, 2004: System-relative distribution of dropsondes during BAMEX and lessons learned. Preprints, 22nd Conference on Severe Local Storms. Paper 5.6.

Bartels, D. L., and R. A. Maddox, 1991: Midlevel cyclonic vortices generated by mesoscale convective systems. Mon. Wea. Rev., 119, 104–118.

Davis, C. A., and S. B. Trier, 2004: Mesoscale convective vortices observed during BAMEX. Part I: Kinematic and thermodynamic structure. Preprints, 22nd Conference on Severe Local Storms. Paper 5.1.

Davis, C. A., and M. L. Weisman, 2004: An overview of the Bow-Echo and MCV Experiment (BAMEX). Preprints, 22nd Conference on Severe Local Storms. Paper 4.1.

Davis, C. A., D. A. Ahijevych, and S. B. Trier, 2002: Detection and prediction of warm season midtropospheric vortices by the Rapid Update Cycle. Mon. Wea. Rev., 130, 24-42.

Fritsch, J. M., J. D. Murphy, and J. S. Kain, 1994: Warm core vortex amplifi cation over land. J. Atmos. Sci., 51, 1780–1807.

Raymond, D. J., and H. Jiang, 1990: A theory for long-lived mesoscale convective systems. J. Atmos. Sci., 47, 3067–3077.

Trier, S. B., and C. A. Davis, 2002: Influence of balanced motions on heavy precipitation within a long-lived convectively generated vortex. Mon. Wea. Rev., 130, 877–899.

Trier, S. B., C. A. Davis, and J. D. Tuttle, 2000: Long-lived mesoconvective vortices and their environment. Part I: Observations from the central United States during the 1998 warm season. Mon. Wea. Rev., 128, 3376–3395.

Weisman, M. L., C. Davis, and J. Done, 2004: The promise and challenge of explicit convective forecasting with the WRF model. Preprints, 22nd Conference on Severe Local Storms. Paper 17.2.